THz QCL Self-Mixing Interferometry for Biomedical Applications

Aleksandar D. Rakić,[a] Thomas Taimre,[b] Karl Bertling,[a] Yah Leng Lim,[a] Stephen J. Wilson,[a] Milan Nikolić,[a] Alexander Valavanis,[c] Dragan Indjin,[c] Edmund H. Linfield,[c] A. Giles Davies,[c] Blake Ferguson,[d] Graeme Walker,[d] Helmut Schaider,[e] and H. Peter Soyer[e]

[a]School of Information Technology and Electrical Engineering, The University of Queensland, Brisbane, QLD 4072, Australia;
[b]School of Mathematics and Physics, The University of Queensland, Brisbane, QLD 4072, Australia;
[c]School of Electronic and Electrical Engineering, University of Leeds, Leeds LS2 9JT, United Kingdom;
[d]Cancer Program, Queensland Institute of Medical Research, Herston, QLD 4006, Australia;
[e]Dermatology Research Centre, The University of Queensland, School of Medicine, Translational Research Institute, Brisbane, QLD 4102, Australia

ABSTRACT

In this paper, we introduce the self-mixing phenomenon in terahertz quantum cascade lasers (THz QCLs) and present recent advancements in the development of coherent THz imaging and sensing systems that exploit the self-mixing effect. We describe an imaging method which utilises the interferometric nature of optical feedback in a THz QCL to employ it as a homodyning transceiver. This results in a highly sensitive and compact scheme. Due to the inherently low penetration depth of THz radiation in hydrated biological tissue, imaging of superficial skin is an ideal application for this technique. We present results for imaging of excised skin tissue, showing high-contrast between different tissue types and pathologies.

Keywords: Terahertz imaging; Laser feedback interferometry; Quantum cascade lasers; Tissue imaging.

1. INTRODUCTION

The imaging of structures within skin is a mainstay of the current diagnosis of pathology. Both low-magnification *in vivo* techniques such as dermoscopy, as well as microscopy of excised tissue are based solely on contrast in the visible spectrum. The potential of skin tissue imaging at terahertz wavelengths for the discrimination between healthy and pathological tissue has been explored in a number of studies.[1–6] Imaging skin in different frequency bands provides complementary information about skin. Terahertz (THz) frequency radiation is particularly well suited for this largely functional, biological imaging due to its sensitivity to water content, as a consequence of high absorption of THz radiation in water.[7–14] Diagnostic features based on the response of tissue in this spectral region have been successfully developed in the research community.[15] However, to date, general adoption of THz radiation for biological applications has been impeded by absence of a compact, robust, inexpensive sensing solution.

Over the past decade the quantum cascade laser (QCL) has established itself as one of the most promising radiation sources for imaging applications at THz frequencies due to its ability to generate high power, coherent, continuous-wave (cw) emission with quantum noise-limited linewidths.[16–24] This makes THz QCLs particularly suited to the development of interferometric THz sensing and imaging systems.[25,26]

In this paper, we introduce the self-mixing (SM) phenomenon in QCLs and then present recent advancements in the development of coherent THz imaging and sensing systems that exploit the SM effect. We present an imaging and tissue analysis scheme in the THz radiation band which exploits the interferometric nature of coherent optical feedback in a THz QCL by employing it as a homodyning transceiver. This results in a highly sensitive and compact sensing technique. We apply this scheme to the imaging of excised tissue, and present a range of high-contrast THz images through different reductions of the information-rich interferometric signals. In these images, clear contrast between different tissue types and pathologies is observed, corresponding to interferometric signal morphology.

Further author information: (Send correspondence to A.D.R.)
A.D.R.: E-mail: rakic@itee.uq.edu.au

Terahertz Emitters, Receivers, and Applications V, edited by Manijeh Razeghi, Alexei N. Baranov, John M. Zavada, Dimitris Pavlidis, Proc. of SPIE Vol. 9199, 91990M · © 2014 SPIE
CCC code: 0277-786X/14/$18 · doi: 10.1117/12.2061433

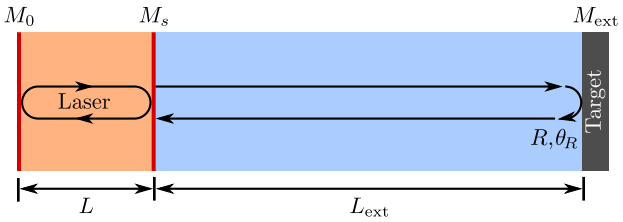

Figure 1. Three mirror model for a laser under feedback. Light recirculates in the laser cavity between mirrors M_0 and M_s — solid arrows in laser cavity of length L. Light exits through M_s, is reflected from the external target M_{ext}, and is reinjected into the laser cavity — solid arrows in external cavity of length L_{ext}.

2. SELF-MIXING PHENOMENON IN THZ QCLS

The SM effect, whereby the re-injection of emitted radiation into the laser cavity affects the laser operating parameters, is remarkably universal, and has been demonstrated in numerous device structures at various wavelengths, including in THz QCLs.[27–36] Whilst this phenomenon can be undesirable in telecommunications targeted for applications, such as communications, it can be exploited for sensing purposes. Indeed, it has been used to measure displacement, velocity, and fluid flow, as well as for coherent and incoherent imaging. It has also been employed to measure the linewidth enhancement factor of semiconductor lasers.[20,37]

The basic structure and operating principles of our SM interferometer are shown in Fig. 1. The re-injected light interferes ("mixes") with the intra-cavity electric field, causing small variations in the fundamental laser parameters including the threshold gain, emitted power, lasing spectrum, and laser terminal voltage.[38–41] Whilst optical feedback affects almost all laser parameters, the two that are most conveniently monitored are the emitted optical power and the voltage across the laser terminals. Of these, monitoring the laser terminal voltage is preferred as it obviates the need for an external THz detector.[42] The small voltage variation (referred to as the "SM signal") depends on both the amplitude and phase of the electric field of the reflected laser beam.

This configuration thus creates a compact, coherent sensor that can probe information about the complex reflectivity or complex refractive index of the external target. The homodyne (coherent) nature of an SM scheme inherently provides very high detection sensitivity, potentially at the quantum noise limit, and therefore a high signal-to-noise ratio can be expected in the SM signal. In the case of THz QCLs, the lifetime of the upper state of the lasing transition is limited by elastic and inelastic scattering mechanisms to a few picoseconds,[43,44] enabling response frequencies of this sensing scheme on the order of tens of GHz.[45–48]

3. TECHNIQUES FOR THZ IMAGING USING LASER FEEDBACK INTERFEROMETRY

Self-mixing signals can be created as a result of temporal variations in optical length of the external cavity (through variation of its refractive index or the physical length), complex reflectivity of the target, or the laser frequency. The imaging process undertaken here involves static objects illuminated by THz radiation; in other words, objects being imaged are not changing during the signal acquisition. Therefore, some type of modulation must be employed in order to generate an SM signal. The laser is typically operated in the cw regime and to create a time-variable interferometric signal one needs to modulate, for example, the laser frequency,[25] reflected beam intensity,[42] or the external cavity length.[49,50]

Here we opt for slow, cw frequency modulation as in Ref. 25, which does not rely on mechanical modulation means, and which results in an SM waveform imprinted with the complex refractive index of the target. To understand these SM signals, we use a three mirror model to describe the laser system under feedback (c.f. Fig. 1),[51] which is equivalent to the steady-state solution to the model proposed by Lang and Kobayashi.[52] In this model, only one round-trip in the external cavity is considered. The phase shift in the external cavity is composed of the transmission phase shift arising from the optical path length as well as the phase change on reflection from the target θ_R. The reflectivity of the target R together with the phase change on reflection form a complex pair which is equivalent to the complex refractive index of the target in terms of the information content.

When the external target is displaced longitudinally, the laser system is swept through a set of compound cavity resonances.[49] The equivalent effect may be obtained by changing the laser frequency, which we accomplish by applying a linear modulation of the laser driving current. The primary effect of this current sweep is a modulation of both the emitted laser power and the voltage developed across the laser terminals. The secondary effect, which is of most importance here, is a linear change of the lasing frequency with current (frequency chirp). This approach in essence constitutes a cw frequency-modulated system for coherently probing the remote target. During the frequency sweep, the SM signal is observed as a set of periodic perturbations embedded in the modulated voltage signal. The temporal separation between the peaks of the SM signal waveform, as well as its shape and phase, depend on the length of the external cavity and the complex reflectivity of the target.[25]

The slow (linear) frequency sweep results in linear dependence of the interferometric phase φ over one frequency modulation period T with time:

$$\varphi(t) = \varphi_0 + \frac{\Phi_\Delta}{T}\, t - \theta_R\,, \tag{1}$$

where φ_0 is the round-trip transmission phase delay in the external cavity at the start of the frequency sweep, Φ_Δ is the interferometric phase deviation caused by the current (frequency) sweep, and θ_R is the phase change on reflection from the material under test (which is assumed not to change significantly with the small frequency sweep). Clearly, φ is a function of the instantaneous laser frequency, which depends on the level of feedback in the laser system.

According to the Lang and Kobayashi model for a semiconductor laser under optical feedback in a steady state,[52] the laser frequency satisfies the phase condition (sometimes called the 'excess phase equation')

$$\varphi_{\mathrm{S}} - \varphi_{\mathrm{FB}} = C\sin(\varphi_{\mathrm{FB}} + \arctan\alpha)\,, \tag{2}$$

where φ_{FB} represents the total external round-trip phase at the perturbed laser frequency, φ_{S} represents the total external round-trip phase at the solitary laser frequency, α is the linewidth enhancement factor,[53,54] and C is the feedback parameter, given by[55–57]

$$C \equiv C(\alpha) = \frac{\tau_{\mathrm{ext}}}{\tau_L}\,\kappa_{\mathrm{ext}}\,\sqrt{1+\alpha^2}\,, \tag{3}$$

where τ_{ext} is the round-trip propagation time in the external cavity, τ_L is the round-trip delay of the solitary laser, and κ_{ext} is the coupling coefficient that depends on the reflectivity of the emitting mirror of the laser R_s and the reflectivity of the target R (associated with mirrors M_s and M_{ext} in Fig. 1, respectively), as

$$\kappa_{\mathrm{ext}} = \varepsilon\sqrt{\frac{R}{R_s}}\,(1-R_s)\ . \tag{4}$$

Here ε represents the fraction of emitted power that is re-injected into the laser cavity, accounting for power loss on transmission in the external cavity and partial re-injection into the laser cavity.

Note that both the solitary phase φ_{S} and the resulting feedback phase φ_{FB} will be of the form in (1) and that we have suppressed the explicit time dependence in (2) for notational simplicity. However, for concreteness, it is useful to think of φ_{S} as the *phase stimulus* varying linearly in time according to (1) and of φ_{FB} as solved from (2) being the resultant feedback phase. Solutions to (2) are not possible in closed form and therefore require numerical solution.[58,59] The interferometric phase change is directly observable through the change in emitted optical power, or equivalently through the change in voltage across the laser terminals.[25,60] In our scheme, the linear current sweep leads to a quasi-linear voltage change near the lasing threshold (referred to as the voltage reference slope) on which the SM signal is superimposed. As such, the SM voltage signal v is related to the phase change through

$$v = V_0 + \beta\cos\left(\varphi_{\mathrm{FB}}\right)\ , \tag{5}$$

where the voltage waveform v is obtained after the removal of a common reference slope to remove the primary effect of the linear current sweep, V_0 is a dc component of this signal (corresponding to a material-dependent voltage offset from the reference slope), and β is the modulation index.[25] For this modulation scheme, note that v is a function of time through its dependence on the interferometric phase φ_{FB} (whose explicit time dependence has been suppressed for notational simplicity).

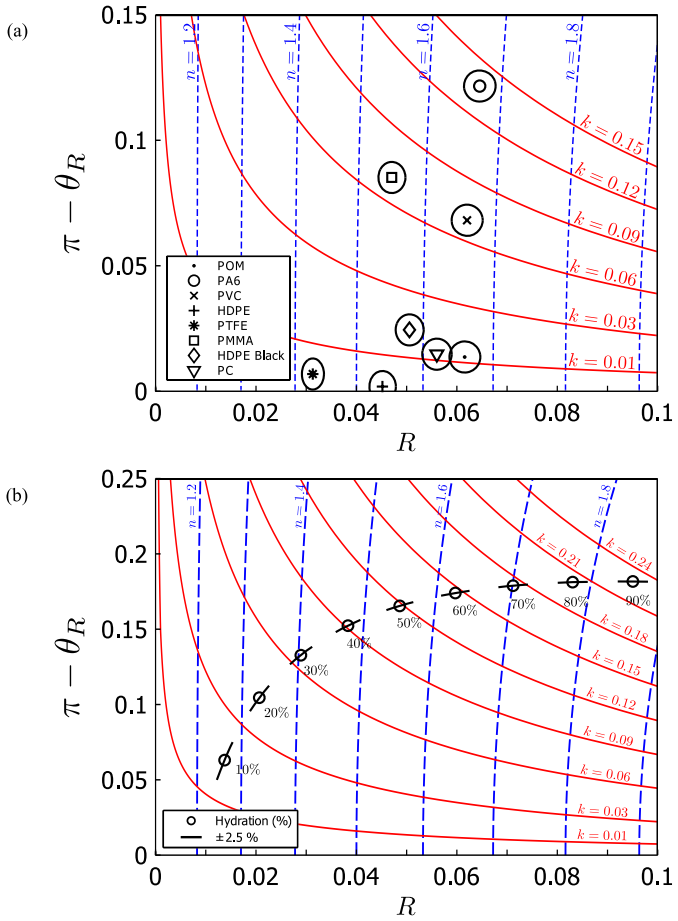

Figure 2. Sensitivity of the system to random variations in $(\sqrt{R}, \theta_R)$. Solid red lines are contours of constant k; broken blue lines are contours of constant n: (a) for a range of organic materials at 2.59 THz, codified through markers with associated 95% confidence intervals.[61] Materials used were: Polyoxymethylene (POM, also known as acetal), nylon 6 (PA6, also known as polycaprolactam), polyvinyl chloride (PVC), high-density polyethylene (HDPE and HDPE Black), polytetrafluoroethylene (PTFE, also known as Teflon), polymethylmethacrylate (PMMA, also known as acrylic), and polycarbonate (PC). (b) The effect of variation in hydration level around each of the circle markers is represented by bars showing the effect of variation in hydration level by $\pm 2.5\%$.

The refractive index n and the extinction coefficient k of the target (the sample being imaged) are equivalent to its complex reflection coefficient [(R, θ_R) pair] (for details see Appendix A). Therefore, change in (n, k) directly affects the SM voltage signal in our model through the phase shift on reflection θ_R appearing in (1), as well as through the reflectivity of the target R appearing in (4).

Typically when an image is obtained it either captures the target surface profile,[50] or variation in optical properties across the target surface.[25,61] The aim of tissue imaging is usually the latter. In that case, it is of interest to determine the influence of variations in optical constants of the target on the complex reflectivity and consequently the SM signal in order to quantify the sensitivity of this sensing scheme, which was discussed in detail in Ref. 61.

Figure 2(a) visualises the relationship between the (n, k) and (R, θ_R) pairs. Lines of constant k (red solid lines) and constant n (blue broken lines) can be used to relate the uncertainties in (R, θ_R) with those in (n, k). From the shape of the constant k lines one can infer that changes in k, especially for low-index materials, result predominantly in changes in θ_R. On the other hand, variations in n translate mainly to changes in reflectivity R. We illustrate this point using an example of eight organic (non-biological) materials with known optical properties at 2.59 THz [shown as different markers in Fig. 2(a), together with 95% confidence intervals in (R, θ_R) space]. The corresponding confidence intervals in (n, k)

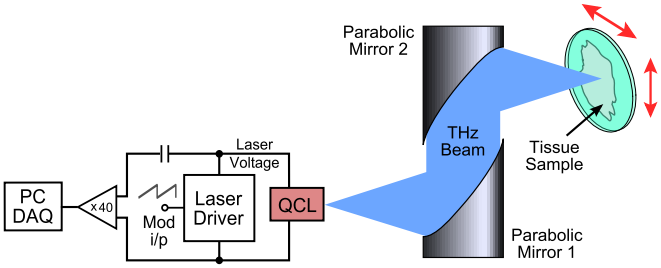

Figure 3. Schematic diagram of the setup used for tissue imaging experiments.

space can be inferred from the (n, k) grid. Materials with similar index (in our figure, POM, PVC, and PA6) have very similar reflection coefficients but the difference in their extinction coefficients clearly translates to difference in their phase shift on reflection.

Figure 2(b) shows the effect of changes in hydration level on the optical properties of skin tissue. The representative markers were calculated using the effective media tissue model from Ref. 14 with hydration as a variable, and with optical constants calculated at 2.59 THz. While we adopted the material model from Ref. 14, our calculations were performed for a simple half-space without considering surface roughness, as opposed to the more elaborate multi-layer model with hydration gradients therein. Sensitivity lines associated with each of the markers in Fig. 2(b) show the effect of variation in hydration level around these representative points on (n, k) and (R, θ_R) pairs. From the locus of the hydration points in these two spaces, it is easy to see that changes in hydration more prominently affect θ_R (resp. k) for low hydration levels and R (resp. n) for high hydration levels. Therefore, to properly image change in hydration level over its full dynamic range, one would greatly benefit from a sensing scheme which concurrently acquires both R and θ_R. The scheme we propose here delivers precisely that.

Furthermore, as mentioned earlier, the value of the (R, θ_R) [resp. (n, k)] pair determines the morphology, amplitude, and the relative position of the time-domain SM waveform. The effect of increasing the real part of the complex refractive index n, results principally in a narrowing of the waveform due to stronger feedback. On the other hand, an increase in the imaginary part of the complex refractive index k predominately translates the waveform whilst leaving its shape unchanged. This effect is mainly due to the strong link between k and θ_R. Thus, the reflection strength and the accompanying phase shift are both encoded (non-linearly) in the morphology, amplitude, and the relative position of the time-domain SM waveform. Due to this intricate mapping of the (R, θ_R) pair onto the highly non-linear SM waveform, we can use a variety of signal processing techniques to successfully extract information about the optical properties of the sample being imaged, with particular choice dependent on the experimental circumstances. In the following sections we will illustrate the application of our technique to image two biological samples: (i) porcine tissue in cross-section and *en face* and (ii) murine skin *en face* at an early stage of malignant melanoma development.

4. EXPERIMENTAL SETUP

Figure 3 shows the schematic diagram of the experimental setup. The THz QCL (operating at 2.59 THz) consisted of a 11.6 µm-thick GaAs/AlGaAs bound-to-continuum active-region that was processed into a semi-insulating surface-plasmon ridge waveguide with dimensions 1.78 mm $\times$ 140 µm. The QCL was mounted onto the cold finger of a continuous-flow cryostat fitted with a polyethylene window and operated at a heat sink temperature of 15 K. Radiation from the QCL was collimated using a 2 inch (50.8 mm) diameter off-axis parabolic reflector with a 4 inch (101.6 mm) focal length and focussed at normal incidence onto the target using a second identical mirror, resulting in an approximately circular beam spot at the focus with $\sim$200 µm $1/e^2$ diameter. The total optical path between the THz QCL source and target was 568.2 mm through an ambient (unpurged) atmosphere.

The laser was driven by a current source at $I_{dc} = 0.43$ A, slightly above the threshold ($I_{th} = 0.4$ A), where the sensitivity to optical feedback is at a maximum.[42,62] A 1 kHz modulating sawtooth current signal (50 mA peak-to-peak amplitude) was superimposed on the dc current resulting in a linear frequency sweep of 600 MHz. Owing to optical feedback from the material under test, the SM waveform containing information about the target is embedded in the

voltage signal measured across the terminals of the QCL. This voltage was amplified by a differential amplifier with 40 times gain and subsequently measured using a 16-bit PC-based data-acquisition (DAQ) card.

For image acquisition, targets were raster-scanned in two dimensions using a two-axis computer-controlled translation stage. The time-domain traces were acquired with spatial resolution of 50 μm, 100 μm, or 200 μm. At each spatial pixel of the target, the voltage signal was recorded as the average of 128 time-domain traces. Therefore the complete set of experimental data contains an array of time-domain waveforms, each corresponding to one spatial pixel on the target.

5. TISSUE IMAGING

Using the experimental apparatus described in Section 4, we performed two sets of tissue imaging experiments using: (i) porcine tissue and (ii) murine skin. For both experiments, a two-dimensional array of time-domain waveforms was acquired, with one waveform associated with each pixel in the image. Experimentally-acquired signals were treated as described in Ref. 25. The resulting interferometric waveforms are information rich, with morphological features such as signal amplitude, peak shape, and peak position containing information about the target. Therefore, there are several ways of reducing this array of time-domain waveforms into an array of numbers, thereby forming images emphasising different features of the target.

Two straightforward reductions were performed for both porcine and murine tissue. The first reduction is characteristic of the total signal strength, calculated as a trimmed sum of the absolute values of signal v, at each spatial pixel and for all measured timepoints. Here, trimmed sum implies an equal proportion (5%) of high and low extremes excluded from the ensemble. This results in a measure capturing reflectivity information about the target. The second is the temporal position of the peak in the trimmed SM signal, relative to the start of the acquisition window — a measure of the relative position of the interferometric peaks within the waveform, and therefore containing predominantly reflection phase information.

5.1 PORCINE TISSUE IMAGE

Figure 4 shows results obtained for the porcine tissue sample, a photograph of which appears in Fig. 4(a). One piece of tissue was placed with its cross-section facing the window [above aluminium separator in Fig. 4(a)]. From the top of this tissue cross-section down to the aluminium separator, the layers of tissue are muscle, fat, and skin. The second piece of tissue was placed *en face* [below aluminium separator in Fig. 4(a)], so that only the surface of the skin was facing the window. Both tissue samples were in excess of 5 mm thick, to effectively ensure no THz reflection from the backing plate.[14]

The image shown in Fig. 4(b) is not a two-dimensional image in the conventional sense. This image represents a vertical slice (1 x 301 pixels) of a high-resolution (50 μm spatial pitch) image of the same sample, indicated by the vertical line in Fig. 4(a). In this image, we display the complete time-domain waveform, with time on the horizontal axis. This representation shows change in waveform morphology as the THz beam moves vertically across the sample, from one type of tissue to another. We can clearly distinguish between fat, muscle, and skin tissue types.

Figures 4(c) and (d) show the two basic reductions explained at the beginning of Section 5, scanned with 200 μm pitch. Contrast between the different tissue types (from top to bottom: muscle; sub-dermal fat; and skin) in the cross-section part of the target (i.e. above the aluminium separator) is clearly visible in the amplitude-like image [Fig. 4(c)], as expected.[10,13] Moreover, in the *en face* part of the target (i.e. below the aluminium separator), clear features are present in both the amplitude-like and the phase-like images [Figs. 4(c) and (d), respectively] that are not evident in the visible image, as can be seen by comparison with the photograph shown in Fig 4(a).

Based on their optical constants, one finds that the reflectivities of tissue and aluminium (used for the triangular marker in Fig. 4) differ by an order of magnitude. Due to the non-linearity in the homodyning process which occurs within the laser cavity, the representation (c) does not properly reflect this fact. However, it expands the dynamic range in the low reflectivity region, when the feedback parameter C is significantly smaller than unity. This representation is useful when the contrast within the imaging frame is known to be small and the amplitude of the SM signal represents the reflectivity well.

On the other hand, with images requiring high dynamic range, where small variations need to be imaged in the presence of a very strong signal in certain areas of the image, other reductions are more appropriate. For example, in Fig. 4(e), we use (trimmed) kurtosis to create the image. Simulations show that, with increased feedback, the interferometric signal acquires

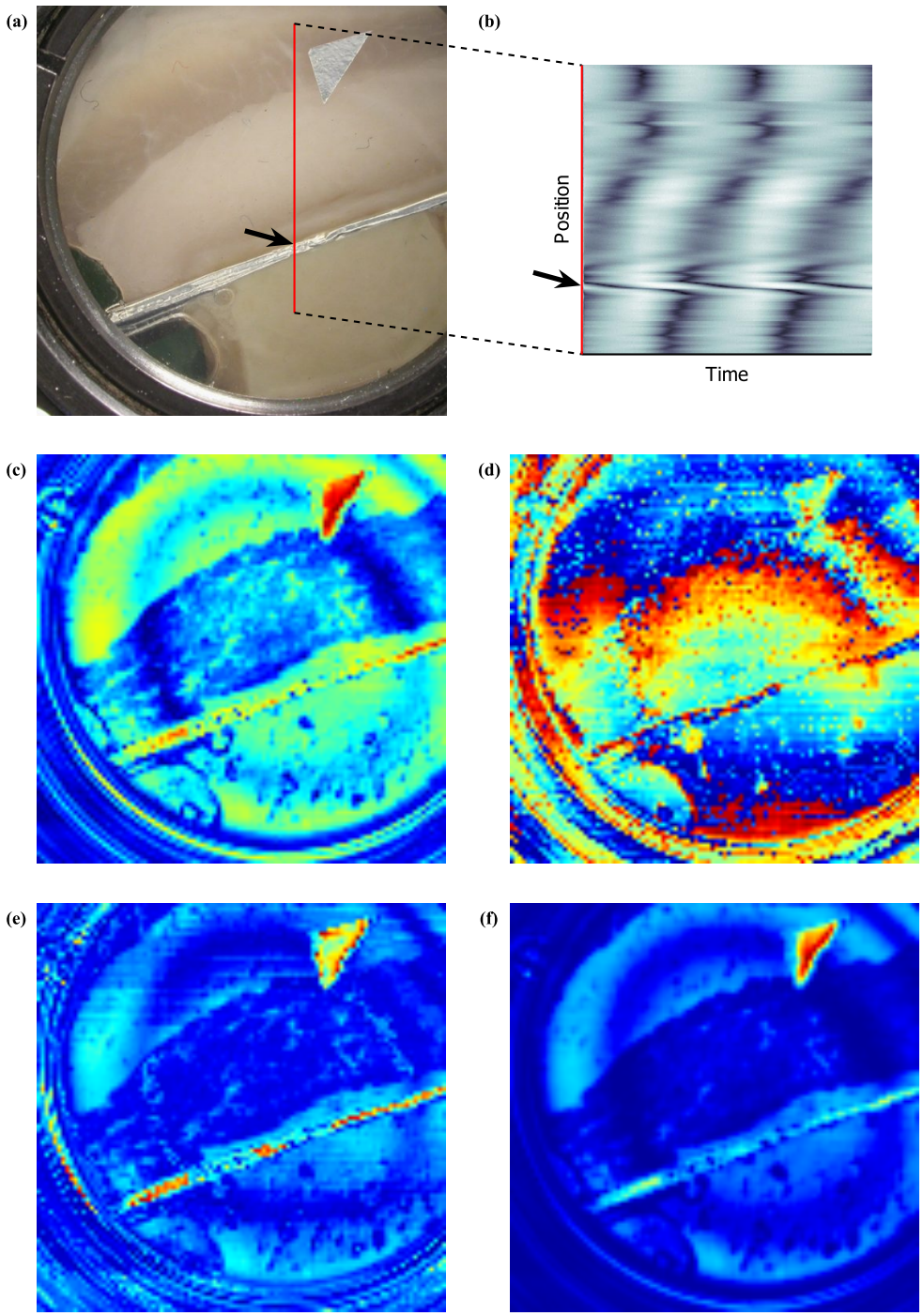

Figure 4. (a) Photograph of the sample; (b) Spatial evolution of time-domain SM waveform; (c) Trimmed total variation; (d) Trimmed last peak position (phase-like); (e) Trimmed kurtosis; (f) Average maximum cross-covariance over immediate neighbours.

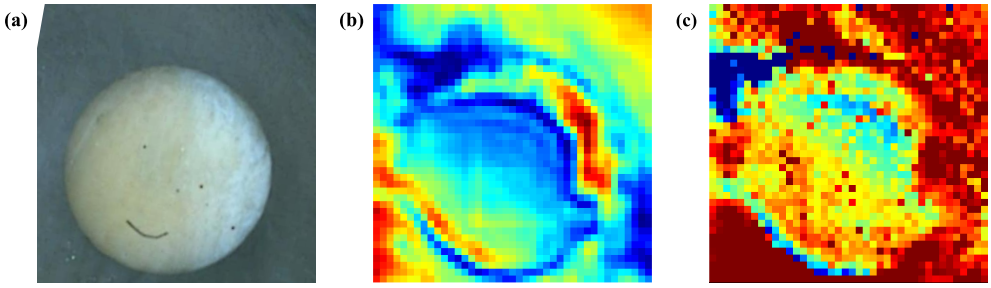

Figure 5. (a) Photograph of the 3 mm diameter skin biopsy from the Cdk4(R24C/R24C)::Tyr-NRAS(Q)(61K) sample; (b) Trimmed total variation; (c) Trimmed last peak position (phase-like).

a shape dominated by narrow peaks, which map to higher values of kurtosis. Therefore, even in the region where signal strength comes into saturation, this reduction properly maps the change in reflectivity over several orders of magnitude of the reflected signal. Skewness and other moment statistics can be used in a similar way. In previous cases, information contained in one waveform was used to create a corresponding pixel in the images. However, one can devise a range of techniques where several neighbouring waveforms can be used together to emphasise particular spatial features of the image. In our example shown in Fig. 4(f) we propose one such scheme where the intensity associated with one pixel is calculated as the average maximum cross-covariance between the time-domain waveform at the pixel of interest and its four cardinal neighbours. We would note that this reduction required no trimming, showing its comparative robustness.

5.2 MURINE MODEL IMAGE

Secondly, we apply our scheme to the reflection-mode imaging of one (3 mm diameter) skin biopsy from the Cdk4 (R24C/R24C)::Tyr-NRAS(Q)(61K) murine model described in Refs. 63 and 64. The sample photographed in Fig. 5(a) shows a barely visible stage 1 melanoma lesion on the left hand side of the sample. Figure 5(b) shows the signal strength reduction of the THz waveforms, while Fig. 5(c) shows the corresponding phase reduction from the array of SM waveforms. The plaque in this sample can be related to features observable in the pair of THz image reductions. The fact that information is contained in both reductions suggests that a signal-strength/phase pair can be associated with different tissue types and pathologies. This points the way towards automatic classification and image segmentation based on the information contained in these reductions.

6. CONCLUSION

In this paper, we discussed the SM phenomenon in THz QCLs and presented recent advancements in the development of coherent THz imaging and sensing systems that rely on the SM effect. This highly sensitive and compact scheme shows promise for biological imaging in the THz frequency range.

Two sets of experimental results were presented. The first set of experiments was performed using excised porcine tissue samples in cross-section and *en face*. The resulting THz images showed clear contrast between different healthy tissue types, and different characteristics in the various image reductions of the information-rich array of SM waveforms, hinting at the potential for tissue classification and clustering. Moreover, the THz images of the *en face* section show clear features which are not apparent in the visible photograph, suggesting that biological imaging with THz radiation augments such imaging in conventional, visible and infra-red spectral bands.

The second set of experiments examined an early stage of murine model for melanoma. The THz images of this early stage sample suggest the possibility for the early detection of changes in the characteristics of skin before they become apparent in visible images. These results of coherent biological imaging at THz frequencies point towards techniques for the discrimination of healthy tissue types for the study of normal physiology and possible therapeutic approaches. Additionally, imaging of skin malignancy in animal models at THz wavelengths shows earlier and potentially more powerful discrimination of lesions than currently possible in visible and IR regions of the electromagnetic spectrum.

APPENDIX A. OPTICAL PROPERTIES OF THE TARGET

We model the optical properties of the target material at a particular spatial point as a (non-magnetic) homogeneous half-space with complex refractive index (using the positive time convention $e^{+j\omega t}$) $\widehat{n} = n - j\,k$ (with $j \equiv \sqrt{-1}$), where n is referred to as the refractive index of the target material, and k is known as its extinction coefficient. Equivalent information is contained in the reflectivity of the material R and the phase shift incurred by THz radiation on reflection θ_R. The dependence of (R, θ_R) on (n, k) is given through the pair of relations[65]

$$R = \frac{(n_0 - n)^2 + k^2}{(n_0 + n)^2 + k^2}\,, \quad \pi - \theta_R = -\arctan\left(\frac{2n_0 k}{n_0^2 - n^2 - k^2}\right)\,, \tag{6}$$

where n_0 is the refractive index of the incident material (typically air), which we take to be $n_0 = 1$ from this point onward. Conversely, the dependence of (n, k) on (R, θ_R) is given through the pair of relations[65]

$$n = \frac{1 - R}{1 + R - 2\sqrt{R}\cos(\theta_R)}\,, \quad k = \frac{2\sqrt{R}\sin(\theta_R)}{1 + R - 2\sqrt{R}\cos(\theta_R)}\,. \tag{7}$$

ACKNOWLEDGMENTS

This research was supported under Australian Research Council's Discovery Projects funding scheme (DP 120 103703) and a Cancer Research UK Leeds Centre Development Fund Equipment award (Grant number C37059/A16369). We also acknowledge support of the ERC 'NOTES' and 'TOSCA' programmes, the Royal Society, the Wolfson Foundation, and the European Cooperation in Science and Technology (COST) Action BM1205. Y.L.L. acknowledges support under the Queensland Government's Smart Futures Fellowships programme.

REFERENCES

[1] Woodward, R. M., Cole, B. E., Wallace, V. P., Pye, R. J., Arnone, D. D., Linfield, E. H., and Pepper, M., "Terahertz pulse imaging in reflection geometry of human skin cancer and skin tissue," *Phys. Med. Biol.* **47**(21), 3853–3863 (2002).

[2] Kim, S. M., Hatami, F., Harris, J. S., Kurian, A. W., Ford, J., King, D., Scalari, G., Giovannini, M., Hoyler, N., Faist, J., and Harris, G., "Biomedical terahertz imaging with a quantum cascade laser," *Appl. Phys. Lett.* **88**(15), 153903 (2006).

[3] Pickwell, E. and Wallace, V. P., "Biomedical applications of terahertz technology," *J. Phys. D: Appl. Phys.* **39**(17), R301–R310 (2006).

[4] Wallace, V. P., Fitzgerald, A. J., Pickwell, E., Pye, R. J., Taday, P. F., Flanagan, N., and Ha, T., "Terahertz pulsed spectroscopy of human basal cell carcinoma," *Appl. Spectrosc.* **60**(10), 1127–1133 (2006).

[5] Taylor, Z. D., Singh, R. S., Culjat, M. O., Suen, J. Y., Grundfest, W. S., Lee, H., and Brown, E. R., "Reflective terahertz imaging of porcine skin burns," *Opt. Lett.* **33**(11), 1258–1260 (2008).

[6] Joseph, C. S., Patel, R., Neel, V. A., Giles, R. H., and Yaroslavsky, A. N., "Imaging of *ex vivo* nonmelanoma skin cancers in the optical and terahertz spectral regions," *J. Biophotonics* **7**(5), 295–303 (2012).

[7] Smye, S. W., Chamberlain, J. M., Fitzgerald, A. J., and Berry, E., "The interaction between terahertz radiation and biological tissue," *Phys. Med. Biol.* **46**(9), R101–R112 (2001).

[8] Fitzgerald, A. J., Berry, E., Zinov'ev, N. N., Homer-Vanniasinkam, S., Miles, R. E., Chamberlain, J. M., and Smith, M. A., "Catalogue of human tissue optical properties at terahertz frequencies," *J. Biol. Phys.* **29**(2–3), 123–128 (2003).

[9] Pickwell, E., Cole, B. E., Fitzgerald, A. J., Pepper, M., and Wallace, V. P., "*In vivo* study of human skin using pulsed terahertz radiation," *Phys. Med. Biol.* **49**(9), 1595–1607 (2004).

[10] He, M., Azad, A. K., Ye, S., and Zhang, W., "Far-infrared signature of animal tissues characterized by terahertz time-domain spectroscopy," *Opt. Commun.* **259**(1), 389–392 (2006).

[11] Xu, J., Plaxco, K. W., and Allen, S. J., "Absorption spectra of liquid water and aqueous buffers between 0.3 and 3.72 THz," *J. Chem. Phys* **124**(3), 036101 (2006).

[12] Huang, S. Y., Wang, Y. X. J., Yeung, D. K. W., Ahuja, A. T., Zhang, Y.-T., and Pickwell-MacPherson, E., "Tissue characterization using terahertz pulsed imaging in reflection geometry," *Phys. Med. Biol.* **54**(1), 149–160 (2009).

[13] Sun, Y., Fischer, B. M., and Pickwell-MacPherson, E., "Effects of formalin fixing on the terahertz properties of biological tissues," *J. Biomed. Opt.* **14**(6), 064017 (2009).

[14] Bennett, D. B., Li, W., Taylor, Z. D., Grundfest, W. S., and Brown, E. R., "Stratified media model for terahertz reflectometry of the skin," *IEEE Sens. J.* **11**(5), 1253–1262 (2011).

[15] Yu, C., Fan, S., Sun, Y., and Pickwell-MacPherson, E., "The potential of terahertz imaging for cancer diagnosis: A review of investigations to date," *Quant. Imaging Med. Surg.* **2**(1), 33–45 (2012).

[16] Köhler, R., Tredicucci, A., Beltram, F., Beere, H. E., Linfield, E. H., Davies, A. G., Ritchie, D. A., Iotti, R. C., and Rossi, F., "Terahertz semiconductor-heterostructure laser," *Nature* **417**(6885), 156–159 (2002).

[17] Barbieri, S., Alton, J., Beere, H. E., Fowler, J., Linfield, E. H., and Ritchie, D. A., "2.9 THz quantum cascade lasers operating up to 70 K in continuous wave," *Appl. Phys. Lett.* **85**(10), 1674–1676 (2004).

[18] Luo, H., Laframboise, S. R., Wasilewski, Z. R., Aers, G. C., Liu, H. C., and Cao, J. C., "Terahertz quantum-cascade lasers based on a three-well active module," *Appl. Phys. Lett.* **90**(4), 041112 (2007).

[19] Belkin, M. A., Fan, J. A., Hormoz, S., Capasso, F., Khanna, S. P., Lachab, M., Davies, A. G., and Linfield, E. H., "Terahertz quantum cascade lasers with copper metal-metal waveguides operating up to 178 K," *Opt. Express* **16**(5), 3242–3248 (2008).

[20] Green, R. P., Xu, J. H., Mahler, L., Tredicucci, A., Beltram, F., Giuliani, G., Beere, H. E., and Ritchie, D. A., "Linewidth enhancement factor of terahertz quantum cascade lasers," *Appl. Phys. Lett.* **92**(7), 071106 (2008).

[21] Khanna, S. P., Chakraborty, S., Lachab, M., Hinchcliffe, N. M., Linfield, E. H., and Davies, A. G., "The growth and measurement of terahertz quantum cascade lasers," *Physica E: Low Dimens. Syst. Nanostruct.* **40**(6), 1859–1861 (2008).

[22] Ravaro, M., Barbieri, S., Santarelli, G., Jagtap, V., Manquest, C., Sirtori, C., Khanna, S. P., and Linfield, E. H., "Measurement of the intrinsic linewidth of terahertz quantum cascade lasers using a near-infrared frequency comb," *Opt. Express* **20**(23), 25654–25661 (2012).

[23] Vitiello, M. S., Consolino, L., Bartalini, S., Taschin, A., Tredicucci, A., Inguscio, M., and De Natale, P., "Quantum-limited frequency fluctuations in a terahertz laser," *Nature Photon.* **6**(8), 525–528 (2012).

[24] Li, L., Chen, L., Zhu, J., Freeman, J., Dean, P., Valavanis, A., Davies, A. G., and Linfield, E. H., "Terahertz quantum cascade lasers with >1 W output powers," *Electron. Lett.* **50**(4), 309–311 (2014).

[25] Rakić, A. D., Taimre, T., Bertling, K., Lim, Y. L., Dean, P., Indjin, D., Ikonić, Z., Harrison, P., Valavanis, A., Khanna, S. P., Lachab, M., Wilson, S. J., Linfield, E. H., and Davies, A. G., "Swept-frequency feedback interferometry using terahertz frequency QCLs: a method for imaging and materials analysis," *Opt. Express* **21**(19), 22194–22205 (2013).

[26] Ravaro, M., Jagtap, V., Santarelli, G., Sirtori, C., Li, L. H., Khanna, S. P., Linfield, E. H., and Barbieri, S., "Continuous-wave coherent imaging with terahertz quantum cascade lasers using electro-optic harmonic sampling," *Appl. Phys. Lett.* **102**(9), 091107 (2013).

[27] King, P. G. R. and Steward, G. J., "Metrology with an optical maser," *New Scientist* **17**(323), 180 (1963).

[28] Donati, S., "Laser interferometry by induced modulation of cavity field," *J. Appl. Phys.* **49**(2), 495–497 (1978).

[29] Churnside, J. H., "Laser Doppler velocimetry by modulating a CO_2 laser with backscattered light," *Appl. Opt.* **23**(1), 61–66 (1984).

[30] Nerin, P., Puget, P., Besesty, P., and Chartier, G., "Self-mixing using a dual-polarisation Nd:YAG microchip laser," *Electron. Lett.* **33**(6), 491–492 (1997).

[31] Han, D., Wang, M., and Zhou, J., "Self-mixing speckle in an erbium-doped fiber ring laser and its application to velocity sensing," *IEEE Photon. Technol. Lett.* **19**(18), 1398–1400 (2007).

[32] Dai, X., Wang, M., Zhao, Y., and Zhou, J., "Self-mixing interference in fiber ring laser and its application for vibration measurement," *Opt. Express* **17**(19), 16543–16548 (2009).

[33] Lim, Y. L., Nikolić, M., Bertling, K., Kliese, R., and Rakić, A. D., "Self-mixing imaging sensor using a monolithic VCSEL array with parallel readout," *Opt. Express* **17**(7), 5517–5525 (2009).

[34] Sudo, S., Ohtomo, T., Takahashi, Y., Oishi, T., and Otsuka, K., "Determination of velocity of self-mobile phytoplankton using a self-mixing thin-slice solid-state laser," *Appl. Opt.* **48**(20), 4049–4055 (2009).

[35] Bertling, K., Lim, Y. L., Taimre, T., Indjin, D., Dean, P., Weih, R., Höfling, S., Kamp, M., von Edlinger, M., Koeth, J., and Rakić, A. D., "Demonstration of the self-mixing effect in interband cascade lasers," *Appl. Phys. Lett.* **103**(23), 231107 (2013).

[36] Valavanis, A., Dean, P., Lim, Y. L., Alhathlool, R., Nikolić, M., Kliese, R., Khanna, S. P., Indjin, D., Wilson, S. J., Rakić, A. D., Linfield, E. H., and Davies, A. G., "Self-mixing interferometry with terahertz quantum cascade lasers," *IEEE Sens. J.* **13**(1), 37–43 (2013).

[37] Yu, Y., Giuliani, G., and Donati, S., "Measurement of the linewidth enhancement factor of semiconductor lasers based on the optical feedback self-mixing effect," *IEEE Photon. Technol. Lett.* **16**(4), 990–992 (2004).

[38] Donati, S., "Developing self-mixing interferometry for instrumentation and measurements," *Laser Photon. Rev.* **6**(3), 393–417 (2012).

[39] Bosch, T., Bès, C., Scalise, L., and Plantier, G., "Optical feedback interferometry," in [*Encyclopedia of Sensors*], Grimes, C. A. and Dickey, E. C., eds., 1–20, American Scientific Publishers (2006).

[40] Giuliani, G., Norgia, M., Donati, S., and Bosch, T., "Laser diode self-mixing technique for sensing applications," *J. Opt. A, Pure Appl. Opt.* **4**(6), S283–S294 (2002).

[41] Giuliani, G. and Donati, S., "Laser interferometry," in [*Unlocking Dynamical Diversity: Optical Feedback Effects on Semiconductor Lasers*], Kane, D. M. and Shore, K. A., eds., John Wiley & Sons, Chichester (2005).

[42] Dean, P., Lim, Y. L., Valavanis, A., Kliese, R., Nikolić, M., Khanna, S. P., Lachab, M., Indjin, D., Ikonić, Z., Harrison, P., Rakić, A. D., Linfield, E. H., and Davies, A. G., "Terahertz imaging through self-mixing in a quantum cascade laser," *Opt. Lett.* **36**(13), 2587–2589 (2011).

[43] Scalari, G., Ajili, L., Faist, J., Beere, H., Linfield, E., Ritchie, D., and Davies, G., "Far-infrared ($\lambda \simeq 87$ μm) bound-to-continuum quantum-cascade lasers operating up to 90 K," *Appl. Phys. Lett.* **82**(19), 3165–3167 (2003).

[44] Indjin, D., Harrison, P., Kelsall, R. W., and Ikonić, Z., "Mechanisms of temperature performance degradation in terahertz quantum-cascade lasers," *Appl. Phys. Lett.* **82**(9), 1347–1349 (2003).

[45] Paiella, R., Martini, R., Capasso, F., Gmachl, C., Hwang, H. Y., Sivco, D. L., Baillargeon, J. N., Cho, A. Y., Whittaker, E. A., and Liu, H. C., "High-frequency modulation without the relaxation oscillation resonance in quantum cascade lasers," *Appl. Phys. Lett.* **79**(16), 2526–2528 (2001).

[46] Barbieri, S., Maineult, W., Dhillon, S. S., Sirtori, C., Alton, J., Breuil, N., Beere, H. E., and Ritchie, D. A., "13 GHz direct modulation of terahertz quantum cascade lasers," *Appl. Phys. Lett.* **91**(14), 143510 (2007).

[47] Gellie, P., Barbieri, S., Lampin, J.-F., Filloux, P., Manquest, C., Sirtori, C., Sagnes, I., Khanna, S. P., Linfield, E. H., Davies, A. G., Beere, H., and Ritchie, D., "Injection-locking of terahertz quantum cascade lasers up to 35 GHz using RF amplitude modulation," *Opt. Express* **18**(20), 20799–20816 (2010).

[48] Barbieri, S., Ravaro, M., Gellie, P., Santarelli, G., Manquest, C., Sirtori, C., Khanna, S. P., Linfield, E. H., and Davies, A. G., "Coherent sampling of active mode-locked terahertz quantum cascade lasers and frequency synthesis," *Nature Photon.* **5**(5), 306–313 (2011).

[49] Lim, Y. L., Dean, P., Nikolić, M., Kliese, R., Khanna, S. P., Lachab, M., Valavanis, A., Indjin, D., Ikonić, Z., Harrison, P., Linfield, E. H., Davies, A. G., Wilson, S. J., and Rakić, A. D., "Demonstration of a self-mixing displacement sensor based on terahertz quantum cascade lasers," *Appl. Phys. Lett.* **99**(8), 081108 (2011).

[50] Dean, P., Valavanis, A., Keeley, J., Bertling, K., Leng Lim, Y., Alhathlool, R., Chowdhury, S., Taimre, T., Li, L. H., Indjin, D., Wilson, S. J., Rakić, A. D., Linfield, E. H., and Giles Davies, A., "Coherent three-dimensional terahertz imaging through self-mixing in a quantum cascade laser," *Appl. Phys. Lett.* **103**(18), 181112 (2013).

[51] Petermann, K., [*Laser diode modulation and noise*], Kluwer Academic Publishers, Dordrecht (1991).

[52] Lang, R. and Kobayashi, K., "External optical feedback effects on semiconductor injection laser properties," *IEEE J. Quantum Electron.* **16**(3), 347–355 (1980).

[53] Henry, C. H., "Theory of the linewidth of semiconductor lasers," *IEEE J. Quantum Electron.* **18**, 259–264 (1982).

[54] Osiński, M. and Buus, J., "Linewidth broadening factor in semiconductor lasers — an overview," *IEEE J. Quantum Electron.* **23**(1), 9–29 (1987).

[55] Acket, G. A., Lenstra, D., den Boef, A. J., and Verbeek, B. H., "The influence of feedback intensity on longitudinal mode properties and optical noise in index-guided semiconductor lasers," *IEEE J. Quantum Electron.* **20**(10), 1163–1169 (1984).

[56] Spencer, P., Rees, P., and Pierce, I., "Theoretical analysis," in [*Unlocking Dynamical Diversity: Optical Feedback Effects on Semiconductor Lasers*], Kane, D. M. and Shore, K. A., eds., John Wiley & Sons, Chichester (2005).

[57] Taimre, T. and Rakić, A. D., "On the nature of Acket's characteristic parameter C in semiconductor lasers," *Appl. Opt.* **53**(5), 1001–1006 (2014).

[58] Kliese, R., Taimre, T., Bakar, A. A. A., Lim, Y. L., Bertling, K., Nikolić, M., Perchoux, J., Bosch, T., and Rakić, A. D., "Solving self-mixing equations for arbitrary feedback levels: a concise algorithm," *Appl. Opt.* **53**(17), 3723–3736 (2014).

[59] Plantier, G., Bes, C., and Bosch, T., "Behavioral model of a self-mixing laser diode sensor," *IEEE J. Quantum Electron.* **41**(9), 1157–1167 (2005).

[60] Lim, Y. L., Bertling, K., Rio, P., Tucker, J. R., and Rakic, A. D., "Displacement and distance measurement using the change in junction voltage across a laser diode due to the self-mixing effect," *Proc. SPIE Int. Soc. Opt. Eng.* **6038**, 60381O (2006).

[61] Taimre, T., Bertling, K., Lim, Y. L., Dean, P., Indjin, D., and Rakić, A. D., "Methodology for materials analysis using swept-frequency feedback interferometry with terahertz frequency quantum cascade lasers," *Opt. Express* **22**(15), 18633–18647 (2014).

[62] Donati, S., "Responsivity and noise of self-mixing photodetection schemes," *IEEE J. Quantum Electron.* **47**(11), 1428–1433 (2011).

[63] Wurm, E. M., Lin, L. L., Ferguson, B., Lambie, D., Prow, T. W., Walker, G. J., and Soyer, H. P., "A blueprint for staging of murine melanocytic lesions based on the Cdk4(R24C/R24C)::Tyr-NRAS(Q)(61K) model," *Exp. Dermatol.* **21**(9), 676–681 (2012).

[64] Chai, E., Ferguson, B., Prow, T., Soyer, P., and Walker, G., "Three-dimensional modelling for estimation of nevus count and probability of nevus-melanoma progression in a murine model," *Pigment Cell Melanoma Res.* **27**(2), 317–319 (2014).

[65] Rakić, A. D., "Algorithm for the determination of intrinsic optical constants of metal films: application to aluminum," *Appl. Opt.* **34**(22), 4755–4767 (1995).